Proceedings of The Fifteenth (2005) International Offshore and Polar Engineering Conference
Seoul, Korea, June 19–24, 2005

ISBN 1-880653-64-8 (Set); ISSN 1098-6189 (Set)

Wave EnergyFocusing in aThree-dimensional Numerical WaveTank

C. Fochesato, F. Dias**, S. Grilli****

* Mathématiques Appliquées de Bordeaux (Université de Bordeaux), Talence, France

** Centre de Mathématiques et de Leurs Applications (Ecole Normale Supérieure de Cachan), Cachan, France

*** Ocean Engineering Department (University of Rhode Island), Narragansett, RI, U.S.A.

ABSTRACT

Directional wave energy focusing in space is one of the mechanisms that may contribute to the generation of a rogue wave in the ocean. To this effect, in this paper, we study the generation of extreme waves in a three-dimensional numerical wave tank from the motion of a snake wavemaker. The numerical model solves incompressible fully nonlinear free-surface Euler equations for potential flow, using a higher-order Boundary Element Method and a mixed Eulerian-Lagrangian time updating. Recent improvements of this numerical model have consisted in the implementation of the Fast Multipole Algorithm, in order to improve the computational efficiency of the spatial solver. A typical case of a near breaking rogue wave is presented as an application. A description of the particular geometry of such a wave is given, as well as preliminary results for the particle velocities at the surface and under the wave crest.

KEY WORDS: numerical wave tank, boundary element method, fast multipole algorithm.

INTRODUCTION

The general framework of this work is the study of the rare but important phenomenon that represent freak waves at sea. Despite their low probability of occurrence, these waves can cause severe damages to ocean structures. Hence, the off-shore and naval communities must take into account loads created by such waves for developing their design rules. Besides their low probability, freak waves are characterized by the fact that they are localized in time as well as in space. They result from a local focusing of wave energy, which may be due to multiple factors. Among these, spatial focusing is one of the most commonly proposed mechanisms to explain the appearance of rogue waves. As a first level approximation, linear theory suggests that different wave components with different phases and directions can superimpose in a small region of space and time and produce a much larger wave. Other factors, however, may cause wave energy focusing, such as bottom topography in shallow water, or wave-current interactions. In deep water and without the presence of a current, a recently proposed mechanism is the modulational instability (Benjamin-Feir instability). Other wave-wave interactions or interactions with atmospheric conditions may also play a role in the phenomenon. These mechanisms are summarized in the recent review article by Kharif and Pelinovsky (2003).

While most studies of rogue waves so far have assumed deep water, it has been shown that these waves can occur for any water depth. In the present study, we consider an arbitrary finite depth, but specify a flat bottom in order to concentrate on one focusing mechanism only. Our model can however feature an arbitrary bottom topography.

Early two-dimensional (2D) studies, both numerical and experimental, used the mechanism of frequency focusing, which occurs when faster waves catch slower ones that have been generated earlier, to create wave superposition. More recently, spatial energy focusing has been the typical mechanism used to generate extreme waves in three-dimensional (3D) wave tank. To do so, a properly programmed snake wavemaker creates the

superposition of several directional sinusoidal wave components. She *et al.* (1994) made such laboratory experiments and studied the kinematics of breaking waves using the PIV technique. Brandini and Grilli (2001) and Brandini (2001) carried out a 3D numerical study of spatial wave focusing, using the Boundary Element model of Grilli *et al.* (2001) and implementing both a snake wavemaker to generate waves at one extremity of a 3D Numerical Wave Tank (NWT), and an open absorbing boundary at the other extremity. More recently, Bonnefoy *et al.* (2004) developed a numerical model based on a higher-order spectral solution of Euler's equations with a free surface, and compared their results with experiments. Although their method cannot model overturning waves, it allows to consider many wave components in a large basin, such as random wave fields with wave components propagating as wave packets. Hence, their method can simulate wave focusing events, very close to those occurring in actual sea states.

By contrast, the goal of the present study is to numerically simulate intense directional energy focusing in a 3D-NWT, leading to wave breaking, and study the kinematics of such extreme waves. Following Grilli and Brandini (2001), we use a Boundary Element model to solve Euler equations with a free surface. The computational cost of their original method, however, which grows quadratically with the discretization, makes these computations rapidly prohibitive. We eliminate this obstacle by implementing the Fast Multipole Algorithm (FMA) to accelerate all the matrix-vector products in the spatial solver (Fochesato and Dias, 2004), and achieve a computational cost almost proportional to the discretization.

First developed by Greengard and Rokhlin (1987) for the N-body problem, the Fast Multipole Algorithm allows a faster computation of all pairwise interactions in a system of N particles, in particular the interactions governed by Laplace's equation. So it is well suited to our problem and we chose to apply this technique. The idea of the algorithm is based on the fact that the interaction strength decreases with distance, so that far points can be grouped together to contribute at one collocation point. A hierarchical subdivision of space gives automatically distance criteria to distinguish close interactions from far ones. The fast algorithm can be used alone to solve Laplace's equation, but it can also be associated with an integral representation of this equation. The discretization then leads to a linear system with matrix-vector products of an iterative solver that can be accelerated by the FMA. Rokhlin (1985) applied this idea to the equations of potential theory. See the review article by Nishimura (2002) on the application of this algorithm for boundary integral equation methods. Water waves computations with multipole accelerated codes exist. Korsmeyer et al. (1993) applied the fast algorithm with a Boundary Element Method through a Krylov-subspace iterative algorithm. Following Rokhlin's ideas, they designed a modified multipole algorithm for the equations of potential theory. First developed for electrostatic analysis, their code has been generalized to become a fast Laplace solver, which subsequently has been used for potential fluid flows. They got

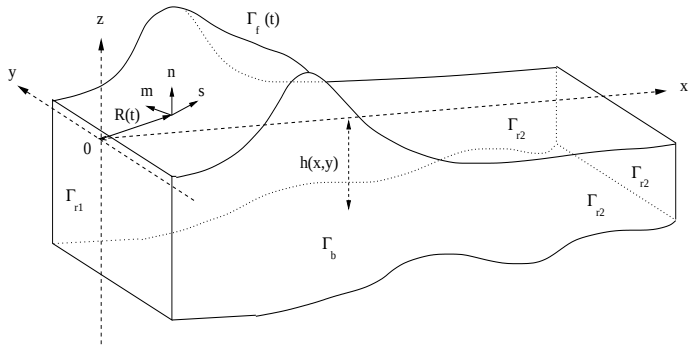

Figure 1: Domain of computation. The free surface $\Gamma_f(t)$ is defined at each time step by the position vector $\boldsymbol{R}(t)$. Lateral boundaries are denoted by Γ_{r1} and Γ_{r2}. The bottom Γ_b is defined by $z = h(x, y)$. Use is made of the Cartesian coordinate system (x, y, z) and of the local curvilinear coordinate system (s, m, n), defined at the point $\boldsymbol{R}(t)$ of the boundary.

an efficient model but the global accuracy is limited by the use of low order elements. Scorpio and Beck (1996) studied wave forces on bodies with a multipole-accelerated desingularized method, and thus did not use boundary elements to discretize the problem. Neither did Graziani and Landrini (1999) who used the Euler-McLaurin quadrature formula in their 2D model. We show briefly below how the Fast Multipole Algorithm can be inserted in the numerical wave tank designed by Grilli et al. (2001) in order to get a more efficient tool. Details can be found in Fochesato and Dias (2004).

For completion, we just note that other fast methods exist for water waves, essentially spectral methods based on the Fast Fourier Transform. In particular, the recent work by Bonnefoy et al. (2004), cited above, is a numerical wave tank for non-breaking waves, that uses a spectral method and also has a O(N) numerical complexity.

The next section presents the numerical method and its more recent improvements. Then the configuration of the NWT is described. Finally, results are presented and discussed for an application.

NUMERICAL MODEL

We consider the equations for a potential flow of an ideal, incompressible fluid, with a free surface. Within the domain, the governing equation is Laplace's equation,

$$\Delta\phi = 0$$

for the velocity potential ϕ, defined from the velocity $\boldsymbol{u} = \boldsymbol{\nabla}\phi$. Green's second identity transforms this equation into a Boundary

Integral Equation (BIE),

$$\alpha(\boldsymbol{x}_l)\,\phi(\boldsymbol{x}_l) = \int_{\Gamma(t)} \left\{ \frac{\partial \phi}{\partial n}(\boldsymbol{x})\, G(\boldsymbol{x},\boldsymbol{x}_l) - \phi(\boldsymbol{x})\, \frac{\partial G}{\partial n}(\boldsymbol{x},\boldsymbol{x}_l) \right\} \mathrm{d}\Gamma, \quad (1)$$

where $G(\boldsymbol{x},\boldsymbol{x}_l) = 1/4\pi|\boldsymbol{x}-\boldsymbol{x}_l|$ is the 3D free space Green's function, $\boldsymbol{n}$ is the normal vector exterior to the boundary and $\alpha(\boldsymbol{x}_l)$ is proportional to the exterior solid angle of the boundary at collocation point $\boldsymbol{x}_l$. On the free surface, the potential ϕ satisfies the nonlinear kinematic and dynamic boundary conditions,

$$\frac{D\,\boldsymbol{R}}{D\,t} = \boldsymbol{\nabla}\phi, \quad (2)$$

$$\frac{D\,\phi}{D\,t} = -gz + \frac{1}{2}\,\boldsymbol{\nabla}\phi\cdot\boldsymbol{\nabla}\phi, \quad (3)$$

where $\boldsymbol{R}$ is the position vector of a fluid particle on the free surface, g the acceleration due to gravity and D/Dt the material derivative. Lateral boundaries are either fixed or moving boundaries. In this study, waves are generated by a wavemaker at the open boundary, $\Gamma_{r1}(t)$, the motion $\boldsymbol{x}_p$ and velocity $\boldsymbol{u}_p$ being specified as,

$$\overline{\boldsymbol{x}} = \boldsymbol{x}_p \;\text{ and }\; \overline{\frac{\partial\phi}{\partial n}} = \boldsymbol{u}_p\cdot\boldsymbol{n}$$

where overlines denote specified values. Along the fixed parts of the boundary, the no-flow condition is prescribed,

$$\overline{\frac{\partial\phi}{\partial n}} = 0.$$

The domain shown in Fig. 1 represents a closed basin such as a wave tank, whose bottom can be defined with arbitrary geometry. The numerical model is presented in detail in Grilli *et al.* (2001) and Fochesato et al. (2005). The time stepping algorithm consists in updating the position vector and the velocity potential on the free surface, based on second-order Taylor series expansions. At each time step, The BIE is solved through the use of a Boundary Element Method. The boundary is divided into elements for which a local interpolation is defined, both for the geometry and field variables. Bi-cubic polynomial shape functions are used and a local change of variables is defined to express the BIE integrals on a curvilinear reference element. The numerical computation of these integrals is performed using a Gauss-Legendre quadrature and appropriate techniques are applied for removing weak singularities of the Green's functions. The number of discretization nodes yields the assembling phase of the discretization matrix. The latter is modified by applying the rigid mode technique, which allows to directly compute the solid angles α in Eq. (1) and thus avoid evaluating the strongly singular integrals of the normal derivative of the Green's function. The use of the multiple node technique, to deal with domain edges and corners also leads to a modification of the algebraic system matrix. The velocity potential, or its normal derivative depending on the boundary condition, is obtained by solving the resulting linear system of equation. Since the system matrix is fully populated and non-symmetric, the method has at best a N^2 computational complexity, where N is the number of nodes in the discretization, when using the iterative algorithm GMRES (optimized conjugate gradient method). Thus the spatial solution at each time step is of the same complexity as the assembling of the system matrix. The FMA is implemented to reduce this complexity when evaluating every matrix-vector in the discretization of the BIE.

The FMA is based on the principle that the Green's function can be expanded in separated variables when the source point $\boldsymbol{x}_l$ and the evaluation point $\boldsymbol{x}$ are far enough from each other on the boundary. Thus, one can write for a point O (origin of the expansion) close to $\boldsymbol{x}$ and far from $\boldsymbol{x}_l$,

$$G(\boldsymbol{x},\boldsymbol{x}_l) \approx \frac{1}{4\pi}\sum_{k=0}^{p}\sum_{m=-k}^{k} \rho^k Y_k^{-m}(\alpha,\beta)\,\frac{Y_k^m(\theta,\varphi)}{r^{k+1}}, \quad (4)$$

where $O\boldsymbol{x} = (\rho,\alpha,\beta)$ and $O\boldsymbol{x}_l = (r,\theta,\varphi)$ in spherical coordinates. Functions $Y_k^{\pm m}$ are the spherical harmonics defined from the Legendre polynomials. In order to determine in which cases this approximation can be used, a hierarchical subdivision of the spatial domain is defined, whose regular partitioning automatically verifies distance criteria. Thus, close interactions are evaluated by direct computation of the Green's functions, whereas far interactions are approximated by successive local operations based on the subdivision into cells and expansions of the Green' functions into spherical harmonics. The underlying theory for this approximation is well established in the case of Laplace's equation. In particular, error and complexity analyses are given in the monograph by Greengard (1988).

In our case, Laplace's equation has been transformed into an integral equation and a specific discretization has been used. Thus, the FMA must be adapted in order to be part of the surface wave model, but the expansions remain the same. The integral Eq. (1) can be written as,

$$\alpha(\boldsymbol{x}_l)\,\phi(\boldsymbol{x}_l) \approx \frac{1}{4\pi}\sum_{k=0}^{p}\sum_{m=-k}^{k} M_k^m(O)\,\frac{Y_k^m(\theta,\varphi)}{r^{k+1}}, \quad (5)$$

where $M_k^m(O)$ is the moment at the origin O,

$$M_k^m(O) = \int_\Gamma \left\{ \frac{\partial\phi}{\partial n}(\boldsymbol{x})\,\rho^k Y_k^{-m}(\alpha,\beta) - \phi(\boldsymbol{x})\,\frac{\partial}{\partial n}\left(\rho^k Y_k^{-m}(\alpha,\beta)\right) \right\} \mathrm{d}\Gamma. \quad (6)$$

Instead of considering mutual interactions between two points on the boundary, we now need to look at the contribution of an element of the discretization to a collocation point. The local computation of several elements grouped together into a multipole relies on a boundary element analysis with the spherical harmonics instead of the Green's function. The integration of the normal derivative of the spherical harmonics is done by taking care of avoiding an apparent singularity, which could generate numerical errors. The discretization by boundary elements only

takes place in the computation of the moments. So the rest of the Fast Multipole Algorithm is unchanged, especially for translation and conversion formulas which allow to pass the information through the hierarchical spatial subdivision, from the multipole contributions to the evaluation at every collocation point. From the surface wave model point of view, we had to adapt all the aspects depending on the existence of the system matrix in the former BEM model. The storage of coefficients that are used several times for each time step, for instance, is now done inside the cells of the hierarchical subdivision. The rigid mode and multiple nodes techniques modified the matrix *a priori* before the computation of the matrix-vector products. They are now considered as correction terms to the result of such products, so that the linear system to be solved keeps the same properties.

The accelerated model benefits from the faster Laplace's equation solver at each time step. The FMA model performance was tested by comparing new results with the former model's results for a 3D application, which requires great accuracy : the propagation of a solitary wave on a sloping bottom with a transverse modulation, and leads to a plunging jet (Grilli et al., 2001). The consistency of the new approximation was checked but, more importantly, the accuracy and stability of results and their convergence with the discretization size was verified. In fact, by adjusting the parameters of the FMA, i.e., the hierarchical spatial subdivision and the number of terms p in the multipole expansions, one can get nearly the same numerical results as with the former model. In this application, for discretizations having more than 4,000 nodes, the computational time was observed to evolve nearly linearly with the number of nodes. See Fochesato and Dias (2004) for detail.

NWT DESCRIPTION

For the idealized applications in this paper, the NWT is defined as a rectangular basin with a flat bottom at depth h_0. Laterally, the NWT is limited by fixed or moving boundaries. At one extremity, a snake wavemaker is implemented (Grilli and Brandini, 2001), as segmented paddles rotating on the bottom at depth $z = -h_0$, with the angular velocity $\dot{\Omega}\,\boldsymbol{j}$. Vertical segments of the wavemaker can move independently, with their position $\boldsymbol{x}_p = (x_p, y_p, z_p)$ defined by,

$$\boldsymbol{x}_p = \boldsymbol{x}_o - \rho\,\boldsymbol{m} \quad \text{, with} \quad \boldsymbol{x}_o = y_p\,\boldsymbol{j} - h_o\,\boldsymbol{k} \tag{7}$$

the coordinates of the paddle axis of rotation. We denote ρ the distance fron the axis of rotation, measured on the wavemaker in the vertical plane. Hence,

$$\rho = \sqrt{x_p^2 + (h_o + z_p)^2} \quad \text{, and} \quad \Omega = \arctan\frac{S_o}{h_o} \tag{8}$$

where $S_o(y,t)$ is the horizontal stroke specified at $z = 0$.

From these definitions, we find the velocity and acceleration vectors on the wavemaker as,

$$\boldsymbol{u}_p = -\dot{\rho}\,\boldsymbol{m} - \rho\,\dot{\Omega}\,\boldsymbol{n}$$

$$\frac{\mathrm{d}\boldsymbol{u}_p}{\mathrm{d}t} = (\rho\,\dot{\Omega}^2 - \ddot{\rho})\,\boldsymbol{m} - (2\,\dot{\rho}\,\dot{\Omega} + \rho\,\ddot{\Omega})\,\boldsymbol{n}. \tag{9}$$

Following Dalrymple (1989), we specify the wavemaker stroke S_o as the linear superposition of N_θ sinusoidal components of amplitude a_n and direction θ_n, as

$$S_o(y,t) = \sum_{n=1}^{N_\theta} a_n \cos\{k_n(y\sin\theta_n - x_f\cos\theta_n) - \omega_n t\} \tag{10}$$

where k_n and ω_n denote the wavenumber and circular frequency of each component, respectively, which are related by the linear dispersion relationship,

$$\omega_n^2 = g\,k_n\,\tanh(k_n h_o) \tag{11}$$

and x_f is the focusing distance for the waves in front of the wavemaker. Angles θ_n are uniformly distributed in the range $[-\theta_{\max}, \theta_{\max}]$. Only directional focusing is studied here, hence $\omega_n = \omega$. Frequency focusing could be specified by adjusting the components' frequency as a function of the angle θ_n. Moreover, for simplicity, we assume the components' amplitudes are identical; different values however could as easily be selected.

The first objective of this work has consisted in finding wavemaker parameter values such that an extreme breaking wave is generated near the middle of the NWT. We thus consider the superposition of ten components having identical properties, but with directions varying between -45 and 45 degrees. The variables being non-dimensionalized (length by the water depth h_0, and time by $\sqrt{h_0/g}$), every component has a frequency $\omega = 1.2816$, which gives a wavelength $L = 2\pi/k = 3.725$ from Eq. (11) and a linear velocity $c = \omega/k = 0.7599$. The amplitude of each individual component is fixed to $a = 0.035$, yielding a steepness of $ka = 0.059$. The energy focusing point is specified at the distance $x_f = 7.5$ from the wavemaker. Once the features of the wave field are defined, the dimensions of the NWT are selected. We choose 10 for the length and 20 for the width of the NWT. At the beginning of the computations, the discretization uses 60 elements in the longitudinal direction, which corresponds to roughly 20 nodes per wavelength. In order to obtain the overturning phase, the resolution is improved to 75 elements from $t \approx 16.25$. The width of the domain is divided into 70 elements, and the depth into 4 elements. [Note that all the boundaries are discretized in the present simulations, unlike in Brandini and Grilli's (2001) work, that used an image method to eliminate the bottom discretization; this simplification will be implemented in future work.]

Figure 2 presents the kind of movement specified by the wavemaker in the NWT. At the other extremity of the domain, an absorbing piston boundary is used (Clement, 1996; Grilli and Horrillo, 1997; Grilli and Brandini, 2001). Though it is not perfectly suited for these intermediate depth waves, it sufficiently delays the instant when reflection cannot be neglected any more to study the extreme 3D breaking wave we are generating in the tank. [The implementation of a piston having the same kind

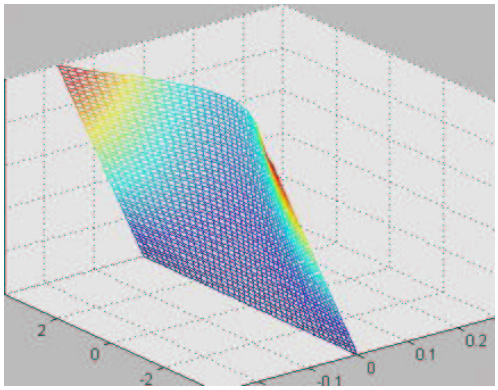

Figure 2: Illustration of the snake movement of the wavemaker located at the left of the tank.

of movement as the snake wavemaker as in Brandini and Grilli (2001) would improve this feature.]

RESULTS

Figures 3, 4 and 5 present the time evolution of the wave field obtained for the wavemaker parameters and NWT discretization discussed in the previous section. Note that only the free surface is shown. The wavemaker progressively sets out, in order to reduce the singularities at the interface between the free surface and the moving boundary (Grilli and Brandini, 2001). We observe, the initially flat free surface at rest starts moving near the wavemaker and a first focused wave of moderate amplitude is generated (Figures 3 and 4). Then, the wave elevation decreases, before disappearing at the plot scale (Figure 4). Hence, the studied mechanism effectively produces some local focusing, transient both in time and space. Behind this first wave, we see a second one which clearly results from the superposition of wave components with different directions (Figures 4(d) and 5(a)). The amplitude of the wavemaker oscillations increases further and the sum of the wave components gives rise to an even larger wave in the middle of the tank (Figure 5(b),(c)). This wave steepens before reaching the focusing area, specified at $x = 7.5$, and we see overturning is initiated at its crest. This is expected as the estimated focal point was based on linear wave theory. At the last time shown for these simulation, the extreme wave crest is located at $x = 4.0$ (Figure 5(d)). Behind this last wave, we see that the phenomenon is starting to be repeated, with a new curved crest line appearing and converging towards the center.

The observation of the free surface shape for this 3D application leads to the following comments. First of all, we see a circular trough located just in front of the wave (the so-called "hole in the sea" reported by freak wave eyewitnesses). Behind it, an even deeper trough has formed, separating the main wave from the curved crest line which follows it. This trough has a crescent shape. A strong asymmetry between the back and the front of the wave is observed. The wave amplitude is significantly larger than that of the following waves which have not yet converged. This asymmetry increases with time and indicates that the wave is about to break. The wave itself appears like a curved front. In the present case where the directionality is important, the front is not so wide and 3D effects are emphasized (note, plot axes are not at real scale).

The properties of this extreme wave, generated in the NWT, agree with geometrical properties of observed freak waves. In particular, Fig. 6 shows a vertical cross-section of the solution obtained at $y = 0$ and $t = 18.051$. We see the wave shape observed in many actual freak wave measurements as well as in earlier 2D numerical studies, for instance those related to modulational instabilities of a wave packet (e.g., Kharif and Pelinovski, 2003): the wave crest amplitude is much larger than the trough amplitudes and the back trough is deeper than the front one. The crest peaks at $z = 0.38$, and the back and front troughs are respectively measured at $z = -0.17$ and $z = -0.10$.

It is remarkable that we get such a 2D characteristic shape, whereas the mechanism of wave generation used here is purely 3D. This suggests some independence of freak wave shapes and properties from the phenomena that have generated it. Figure 7 shows a slice of the solution at the final time $t = 18.355$, when the wave is overturning.

Velocity and acceleration fields computed on the free surface (see Guyenne and Grilli, 2003, for detail) show two main phases in the evolution of this focused wave event. The first phase is one of approach, where the different wave components form a crest line are converging to a point. The obtained kinematics simply corresponds to the features of the propagation of a curved crest line. The second phase corresponds to the appearance of a unique focused wave, resulting from the superposition of the many components. The maximum value of the longitudinal velocity component increases and the largest velocities concentrate more and more at the crest, indicating flow convergence. So this crest tends to go forward, faster than its basic wave components, thus initiating wave breaking. At the same time, the transverse component of the velocity and acceleration fields show that 3D effects are reduced near the wave front face. Hence, the dynamics of imminent breaking of the freak wave takes an almost 2D configuration. [This observation has important implications for the design of offshore structures that would be located in the path of such a wave.] This is in good agreement with some description of a "wall of water", that we can find in stories about extreme wave events in the ocean.

An illustration of results obtained for the wave kinematics at some internal points in a vertical cross-section at $y = 0$ under the wave crest and in the plunging jet is given by Figures 8 and 9.

CONCLUSIONS

This paper presents a summary of the numerical method used to study the mechanism of directional wave energy focusing in a numerical wave tank. The numerical model is based on the solution of incompressible Euler's equations with a free surface for a potential flow, using a Boundary Element Method. Its more recent improvement are presented, in particular, the use of the Fast Multipole Algorithm in order to compute faster every matrix-vector

product coming from the discretization. This allows to overcome the main drawback of such numerical methods, that is its computational complexity which is normally $O(N^2)$. The single application presented consists in generating an extreme wave event by the movement of a snake wavemaker in the NWT. Properties of the generated extreme waves are briefly discussed (shape and kinematics).

Brandini and Grilli (2001) presented a similar study based on an earlier version of this model/NWT. They could not however, reach the overturning phase for an extreme wave event, both due to limitations in the model implementation (now corrected; see Fochesato et al., 2005) and discretization size that could be realistically used. Here, we observe that a vertical 2D slice in the solution under the extreme wave crest looks quite similar to the characteristic shape observed for freak waves in the ocean. The 3D wave generation yields a curved wave front, before focusing occurs, with a circular trough in front of the wave, followed by a deeper trough with a crescent shape. The kinematics shows two main phases. First, we observe the propagation of a curved crest line converging to one narrow area of the NWT. When the focused wave is generated, it steepens and the velocity and acceleration vectors on the front face of the wave have weak transverse components. Therefore, after the focusing phase, the occurrence of wave breaking seems essentially similar to 2D wave dynamics. This corresponds to the aspect of a "wall of water", which appears in some stories of rogue waves in the ocean. Here, the maximal value of the velocity in the crest during overturning (at $t = 18.355$) is $1.1\sqrt{gh_0}$, where g is is the acceleration due to gravity and h_0 the depth of the tank at rest. More details will be given during the conference.

REFERENCES

Broeze J. (1993) "Numerical modelling of nonlinear free surface waves with a three-dimensional panel method." *PhD thesis, University of Twente, Enschede, The Netherlands*.

Bonnefoy F., Le Touze D., and Ferrant P. (2004) "Generation of fully-nonlinear prescribed wave fields using a high-order spectral method," *Proc. 14th Offshore and Polar Engng. Conf.* (ISOPE 2004), Toulon, France, vol. III, 257–263.

Brandini C. (2001) *Nonlinear interaction processes in extreme wave dynamics*, Ph.D. Dissertation, University of Firenze.

Brandini C. and Grilli S. (2001) "Modeling of freak wave generation in a 3D-NWT," *Proc. 11th Offshore and Polar Engng. Conf.* (ISOPE 2001), Stavanger, Norway, Vol III, 124–131.

Clément A. (1996) "Coupling of two absorbing boundary conditions for 2D time-domain simulations of free surface gravity waves," *J. Comp. Phys.*, **26**, 139–151.

Dalrymple R.A. (1989) "Directional wavemaker theory with sidewall reflection," *J. Hydraulic Res.*, **27** (1), 23–34.

Fochesato C. and Dias F. (2004) "Numerical model using the Fast Multipole Algorithm for nonlinear three-dimensional free-surface waves," (preprint CMLA).

Fochesato, C., Grilli, S. and Guyenne P. (2005) "Note on non-orthogonality of local curvilinear co-ordinates in a three-dimensional boundary element method," *Intl. J. Numer. Meth. In Fluids* (in press).

Graziani G., Landrini M. (1999) "Application of Multipoles Expansion Technique to Two-Dimensional Nonlinear Free-Surface Flows," *J. Ship Research.* **43**, 1–12.

Greengard L. (1988) *The Rapid Evaluation of Potential Fields in Particle Systems*, MIT Press, Cambridge, MA.

Greengard L., Rokhlin V. (1987) "A fast algorithm for particle simulations," *J. Comput. Phys.* **73**, 325–348.

Grilli S., Guyenne P., and Dias F. (2001) "A fully nonlinear model for three-dimensional overturning waves over arbitrary bottom," *Int. J. Num. Meth. Fluids*, **35**, 829–867.

Grilli S.T. and Horrillo J. (1997) "Numerical Generation and Absorption of Fully Nonlinear Periodic Waves," *J. Engng. Mech.*, **123** (10), 1060–1069.

Guyenne, P. and Grilli, S.T. (2003) "Numerical study of three-dimensional overturning waves in shallow water", *J. Fluid Mechanics* (submitted).

Kharif C. and Pelinovsky E. (2003) "Physical mechanisms of the rogue wave phenomenon," *Eur. J. Mech. B-Fluids*, **22** (6), 603–634.

Korsmeyer F.T., Yue D.K.P., Nabors K. (1993) "Multipole-Accelerated Preconditioned Iterative Methods for Three-Dimensional Potential Problems," presented at *BEM 15*, Worcester, MA.

Nishimura, N. (2002) "Fast multipole accelerated boundary integral equation methods," *Appl. Mech. Rev.* **55**, 299–324.

Rokhlin V. (1985) "Rapid solution of integral equations of classical potential theory," *J. Comput. Phys.* **60**, 187–207.

Scorpio S., Beck F. (1996) "A Multipole Accelerated Desingularized Method for Computing Nonlinear Wave Forces on Bodies," presented at *15th Intl. Conf. Offshore Mech. Arctic Engng.*, Florence, Italy.

She K., Greated C.A., and Easson W.J. (1994) "Experimental study of three-dimensional wave breaking," *J. of Am. Soc. C. E.*, **120**, 20–36.

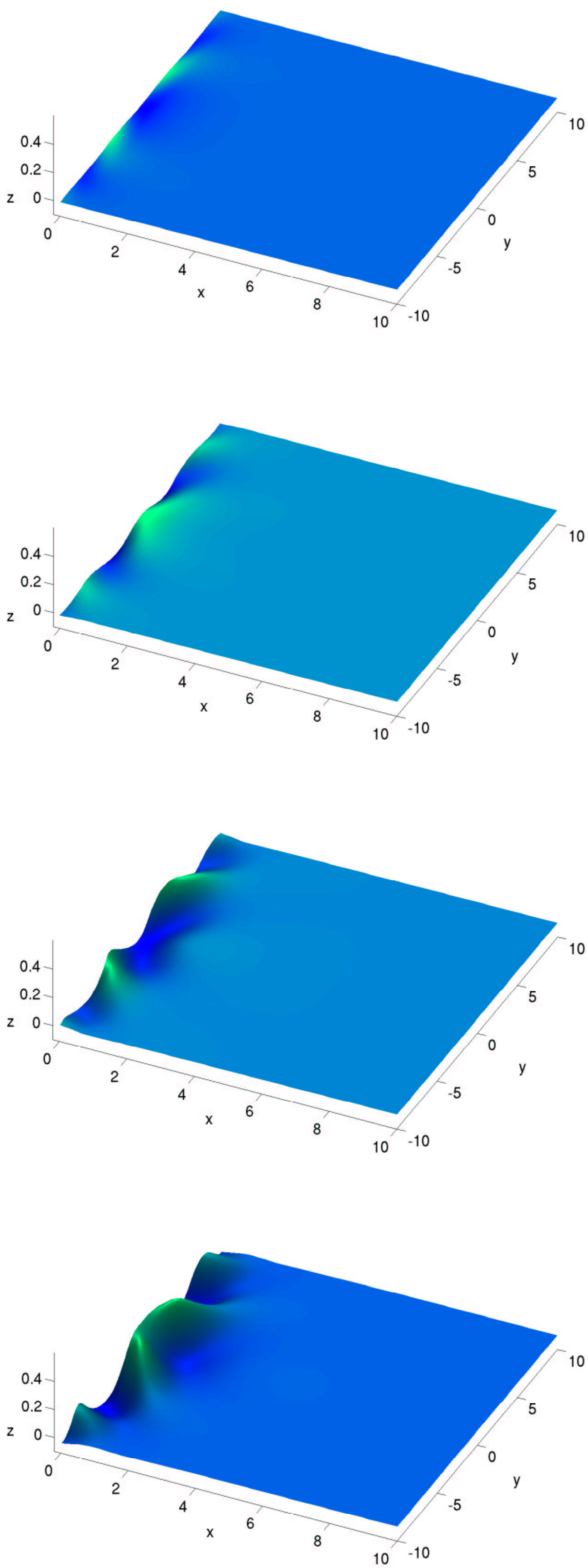

Figure 3: Free surface evolution : (a) at $t = 2.204$, (b) at $t = 4.349$, (c) at $t = 6.363$, (d) at $t = 8.142$,

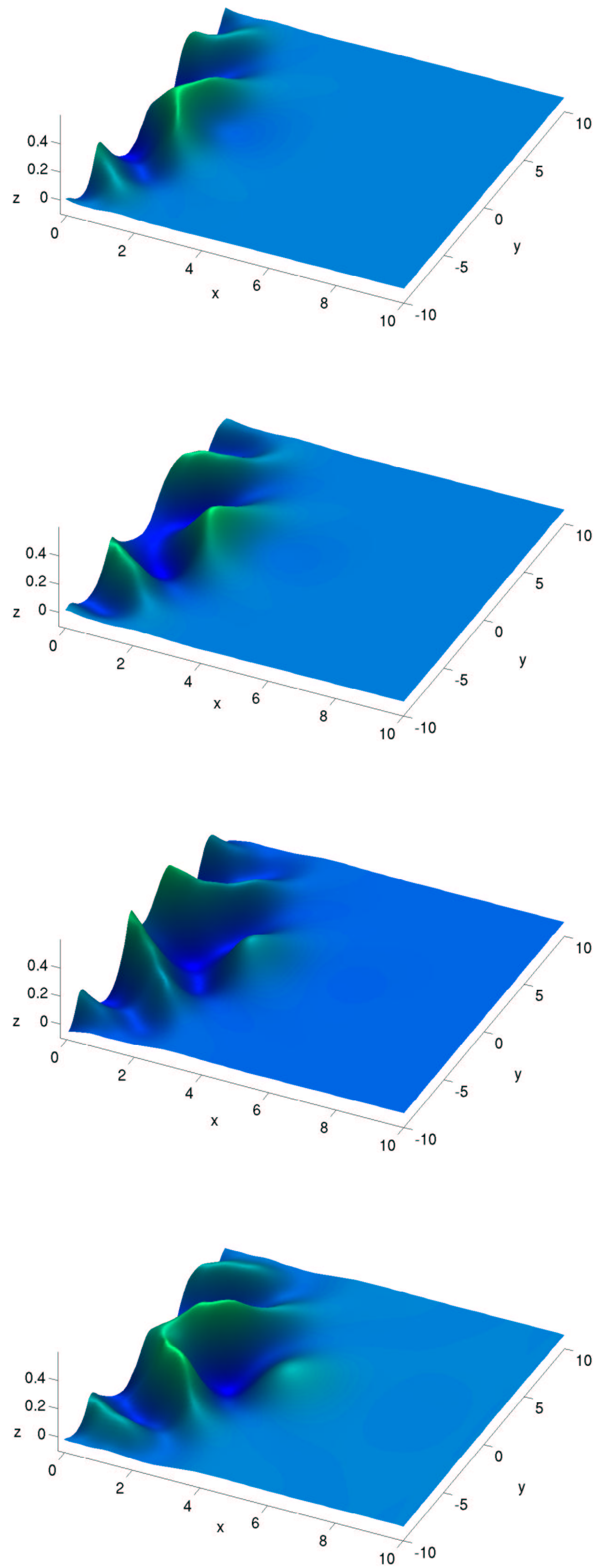

Figure 4: Second part of free surface evolution : (a) at $t = 9.528$, (b) at $t = 10.958$. (c) at $t = 12.498$, (d) at $t = 13.874$,

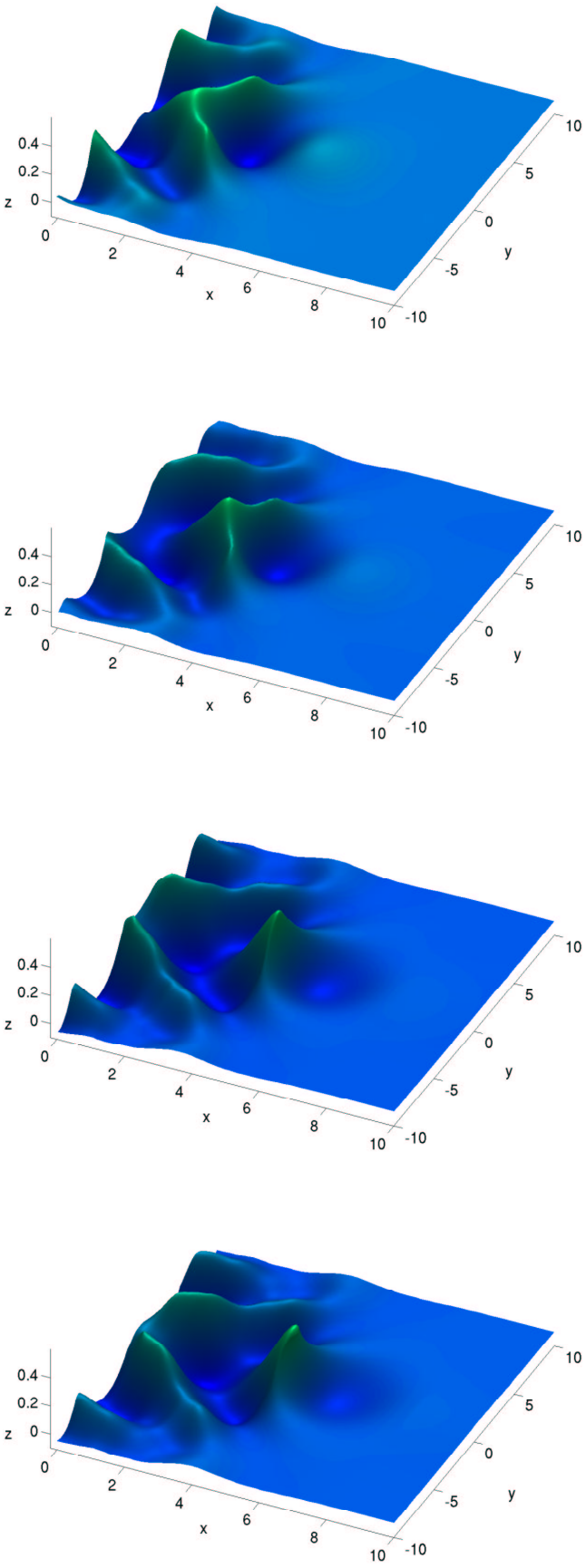

Figure 5: Last part of free surface evolution : (a) at $t = 15.113$, (b) at $t = 16.250$, (c) at $t = 17.839$, (d) at $t = 18.355$.

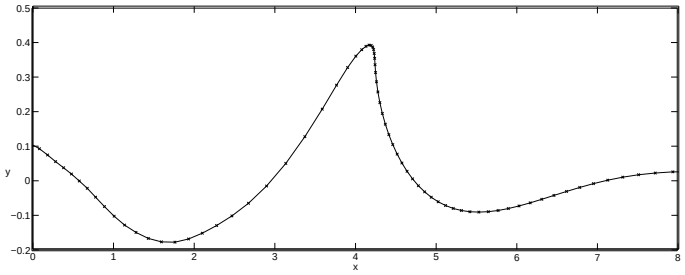

Figure 6: Vertical slice of the free surface at $y = 0$ and $t = 17.8386$.

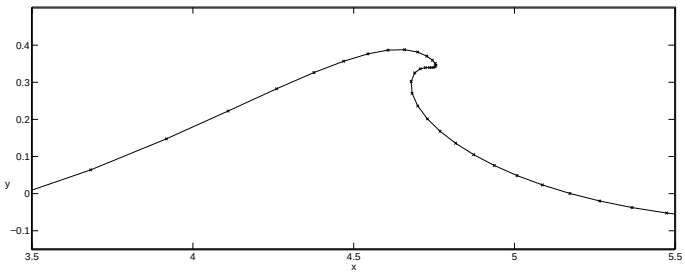

Figure 7: Vertical slice of the free surface at $y = 0$ and $t = 18.355$.

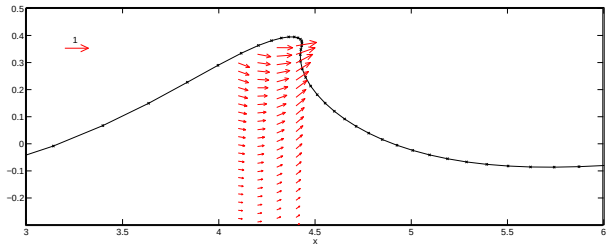

Figure 8: Vertical slice of the free surface at $y = 0$ and $t = 18.051$. Projection of some velocity vectors on the plane $y = 0$, situated under the wave crest. Unit vector used for visualization is also shown.

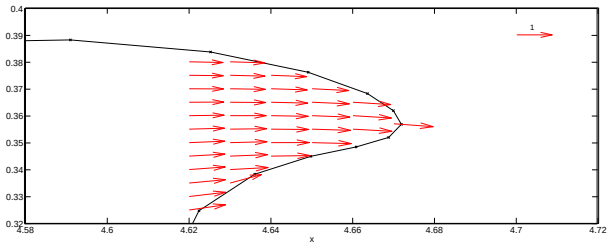

Figure 9: Vertical slice of the free surface at $y = 0$ and $t = 18.279$. Projection of some velocity vectors on the plane $y = 0$, situated in the plunging jet. Unit vector used for visualization is also shown.